PREPARATION AND CHARACTERIZATION OF PVA/ZnO NANOCOMPOSITE

ELHAM GHAROY AHANGAR[1,2], MOHAMMAD HOSSEIN ABBASPOUR-FARD[1,4], NASSER SHAHTAHMASSEBI[2,3], MEHDI KHOJASTEHPOUR[1] and PARISA MADDAHI[2,3]

[1]Biosystems Engineering Department, Faculty of Agriculture, [2]Nanoresearch Centre, [3]Physics Department, Ferdowsi University of Mashhad, Mashhad 9177948974, Iran

[4]Corresponding author.
TEL: +98-915-516-1510;
FAX: +98-511-879-6843;
EMAIL: abaspour@um.ac.ir

Received for Publication April 16, 2014
Accepted for Publication July 31, 2014

doi:10.1111/jfpp.12363

ABSTRACT

ZnO nanoparticles were synthesized by the sol-gel method. The nanoparticles were added to polyvinyl alcohol (PVA) biopolymer to compare the microstructural, mechanical, antibacterial and physical properties of bionanocomposite films reinforced with various loading contents (1, 3 and 5 wt %) and thicknesses (70, 100 and 130 μm). Results showed that with increasing ZnO content to 3 wt %, the tensile strength and Young's modulus increased by 64 and 72%, respectively. The least amount of water vapor permeability was also observed in the sample containing 5 wt % ZnO nanoparticles. Moreover, the antibacterial properties of the films improved with ZnO addition and increased by increasing nanoparticle content up to 5 wt %. However, the transparency of the PVA-based films decreased by ZnO addition.

PRACTICAL APPLICATIONS

A suitable food packaging can increase the shelf life of a food product in addition to sustain its initial quality. The majority of materials used for food packaging are made of undegradable fossil fuel products which have led to the serious environmental problems. On the other hand, the biodegradable films that have been developed suffer from several limitations such as frangibility due to low mechanical strength and weak gas exchange inhibition. Because of very high "surface to volume ratio" of nanostructured materials, their properties are drastically different from common conventional materials. Zinc oxide (ZnO) nanostructured materials have exhibited fascinating properties which have led to wide variety of applications including biomaterial applications. In this regard, the production of the hydrogen peroxide at their surface results in outstanding antibacterial activity. Furthermore, because of ZnO biocompatibility, it is a promising candidate for substitution of silver-based nanoparticles in food packaging applications. Polyvinyl alcohol (PVA), a degradable polymer, is easily dissolved in water, and combination of ZnO nanoparticles and PVA results in improved electrical, mechanical and optical properties. This no poisoning biodegradable nanocomposite should be used as a more effective and environmentally friendly material for food stuff packaging.

INTRODUCTION

In order to protect the foods against microbes and oxidation, the application of appropriate packaging techniques is essential. A suitable packaging should increase the durability of a food product, in addition to sustain its initial quality. Nowadays, the majority of materials used for food packaging are made of undegradable fossil fuel products which have led to serious environmental problems (Tharanathan 2003). In recent decades, the biodegradable films have been developed and studied by numerous research groups but their applications in food packing

industry suffer from several limitations such as frangibility due to low mechanical strength and weak gas exchange inhibition (Vaidya and Bhattacharya 1994).

The development of nanostructured materials for application in nanoscale devices has considerably been expanding. Because of the "surface to volume ratio" enhancement and quantum confinement, the properties of nanomaterials are drastically different from their bulk counterparts (Chaudhry *et al.* 2008). Moreover, the use of polymer nanocomposites (polymer matrices reinforced by nanomaterials) in food packaging has raised considerable attention due to the unique properties of nanomaterials (Arora and Padua 2010). The presence of nanoscaled additives in polymer matrix has been proved to enhance the thermal and mechanical properties and reduce the humidity and gas permeability (Sorrentino *et al.* 2007; Chandrakala *et al.*, 2012).

In this regard, zinc oxide (ZnO) nanostructured materials have gained much of interest as it shows fascinating electrical and optical properties which have led to wide variety of applications from electronics and solar cells to biomedical application (Nair *et al.* 2011). Moreover, the production of the hydrogen peroxide at its surface results in outstanding antibacterial activity (Sawai *et al.* 1998). Furthermore, because of ZnO biocompatibility, it becomes a promising candidate for substitution of silver-based nanoparticles in food packaging applications (Dastjerdi and Montazer 2010).

Different methods can be applied to synthesis ZnO, including: sol-gel (Lee *et al.* 2009), hydrothermal (Suchanek 2009) and laser evaporation technique (Shall *et al.* 1995). Among them, the sol-gel process is a simple and cost-effective method in which the high-purity product can be obtained; this has made it a popular method for the synthesis of nanomaterials (Livage *et al.* 1988).

Polyvinyl alcohol (PVA), a degradable polymer, is easily dissolved in water, and combination of ZnO nanoparticles and PVA results in improved electrical, mechanical and optical properties (Roy *et al.* 2013). In a study, the effect of ZnO nanoparticles on the physical, mechanical and antibacterial properties of pediocin nanofilm was examined, which indicated that the addition of ZnO nanoparticles can enhance the properties of the film (Espitia *et al.* 2013). In a similar research, it was revealed that the insertion of ZnO nanorods resulted in improvements of physical, chemical and antibacterial properties of sago starch films (Nafchi *et al.* 2012). In another study, the mechanical, thermal and antibacterial properties of waterborne polyurethane with addition of flower-like ZnO were recovered (Xue and Wei 2009).

Although several reports on ZnO-based nanocomposite biopolymers have appeared in the literature, it seems that a few of them focused on PVA, which is a degradable polymer suitable for food packaging. Thus, in the present study, ZnO nanoparticles were synthesized via sol-gel method. Furthermore, the microstructure, mechanical, antibacterial, physical and optical properties of PVA nanocomposites were compared as a function of nanoreinforcements in filler loading contents and under the same preparation conditions.

MATERIALS AND METHODS

Materials

Zinc nitrate ($Zn(NO_3)\cdot 6H_2O$), ethanol and sodium chloride (NaCl) were purchased from Scharlau, Barcelona, Spain. Glycerol, PVA (V2000), yeast, agar and tryptone were the procurement of Merck Company, Darmstadt, Germany.

Sample Preparation

Synthesis of Nanomaterials. The so-called sol-gel method was employed for synthesis of ZnO nanoparticles (Kompany *et al.* 2012). The sol was prepared by solving $Zn(NO_3)\cdot 6H_2O$ (as Zn source) in ethanol and distilled water (1:1) as solvent. Subsequently, the ethylene glycol (as polymerization agent) and acetic acid (as complexing agent) (1:1) were added. The homogenous mixture was maintained under reflex at 100–110C for 5 h. After the vaporization of solvent, the gel was produced. The result of light brown powder was calcinated at 500C for 1 h to remove all organic compounds and other impurities to obtain purified ZnO nanopowder.

Nanocomposite Film Fabrication. The solution casting method was used for the fabrication of nanocomposite films. PVA was dissolved in distilled water (3 wt %) at 70–80C. To enhance the film flexibility, glycerol (1 wt %) was added to the solution. Then ZnO nanoparticles were added with different concentrations as 1, 3 and 5 wt %. The mixture was maintained under stirring for 24 h. Ball mill (MM400, Hann., Retsch Lab Equipment, Münden, Germany) was used with 10 Hz for 10 min to homogenize the solution. Then for the effect thickness, the solution with a certain amount was poured in Petri dishes and dried in air. Nanocomposites were prepared and stored as previously described.

Characterization

X-Ray Diffraction Characterization. The crystal structures of the ZnO nanoparticles and nanocomposite film were studied by X-ray diffraction (XRD) (D8 Advance Bruker, Bruker AXS Beijing Office, Beijing, China) technique. The patterns were taken using X-ray diffractometer (Cu Kα line $\lambda = 0.15406$ nm). The intensity was determined

in the range of $10° < 2\theta < 70°$ with 0.04° step size. The Scherrer equation was used to determine the average crystallite size as (Azam *et al.* 2010)

$$D = \frac{K\lambda}{\cos} \quad (1)$$

where D, K, λ, β and θ are the average crystallite (nm), constant factor, X-ray wavelength, full width at half height and scattering angle, respectively.

Chemical Compound Study. The Fourier transmission infrared (FTIR) spectrophotometer (FTIR AVATAR) in the wavelength range of 400–4,000 cm^{-1} was used to study the chemical bonding of samples.

Morphological Analysis. The morphology of ZnO nanoparticles and film surface was examined by transmitted electron microscopy (TEM) (Leo 912AB, Zeiss SMT, Oberkochen, Germany) and scanning electron microscopy (SEM) (Leo 1450VP, Zeiss, Wetzlar, Germany), respectively. In addition, a particle size analyzer (Vasco3, Cordouan Technologies, Pessac, France) was employed for the determination of particle size distribution.

Film Thickness Measurement. A manual digital micrometer (0.01 mm, Qingdao Tide Machine Tool Supply Co., Ltd., Shandong, China) was employed to measure the thickness of the films. For thickness measurements, the samples of the films have all equal size of 7.5×2.0 cm^2. The average thickness of the samples was calculated from five measurements (replications) in different parts of the sample and subsequently used for further calculation of mechanical properties.

Mechanical Properties. The mechanical properties of the samples including tensile strength (TS), elongation (E%) and Young's modulus (YM) at the break were evaluated according to ASTM Standard Method D882-02 (ASTM, 2002) by employing an Instron material testing machine (H5 KS, Manchester, U.K.). The distance between the two jaws of the apparatus was chosen as 5 cm and the strain rate was 50 mm/min (Abdollahi *et al.* 2013). All tests were performed with five replications.

Water Vapor Permeability. The water vapor permeability (WVP) of the samples was tested according to the ASTM E96-92 as explained by Alboofetileh *et al.* (2013). The film was sealed on the top of a glass permeation cell containing distilled water (100% relative humidity (RH); 2.37×10^3 Pa vapor pressure at 20C), placed in a desiccator, which was maintained at 20C and 1.5% RH (28.044 Pa water vapor pressure) with silica gel, and air was stirred in the desiccators. In short, the weight loss due to the vapor transformation through the films was measured for 8 h with 1 h time step. Then the slope of the weight loss versus time was determined by linear regression. The following equation was used to calculate the WVP:

$$WVP = WVTR \times L/P \quad (2)$$

where $WVTR$, L and P are the water vapor transmission rate ($g\ m^2/s$) of the film, the average film thickness (m) and the water vapor pressure difference (Pa) on both sides of the film, respectively. WVP measurements were replicated three times.

Antibacterial Assays. The bactericidal activity of the films was evaluated by a typical agar diffusion test (Tankhiwale and Bajpai 2012). The film's antibacterial effect was assessed by the inhibition zone against *Escherichia coli*. The culture containing lysogeny broth (LB) with sodium chloride for sterilization was autoclaved at 121C for 20 min to reach this object. Then bacteria (10^8 cfu/mL) were cultured with lawn method and incubated at 37C to initiate the bacteria growth. Nanofilms added to the culture containing the bacteria were incubated at 37C for 48 h to achieve bacteria disintegration interval. The zone area surrounding the nanofilm was determined by use of ARCGIS 9.3 (ESRI, Redlands, CA).

Color and Opacity of the Films. The color of the films was determined by the method mentioned in the other studies (Sedaghat and Zahedi 2012). In order to evaluate the quality of film's color, their images with JPEG format were taken using a camera (Nikon Coolpix, Nikon Corporation, Iran Branch, Tehran, Iran). Then the area of interest with 500×500 pixels of the images was isolated and imported to MATLAB software (The MathWorks, Inc., Natick, MA). The RGB color parameters of the images were then converted to L^*(lightness), a^*(red/green) and b^*(yellow/blue). The color difference (ΔE) was calculated with respect to standard plate parameters ($L = 94.63$, $a = -0.88$, $b_0 = 0.65$) (Alboofetileh *et al.* 2013) by using the following equation:

$$\Delta E = \sqrt{(L^* - L)^2 + (a^* - a)^2 + (b^* - b)^2} \quad (3)$$

The light absorption of the films (in the wavelength of 600 nm) was tested in order to evaluate their transparency. The transparency can be quantified via opacity which is calculated from Eq. (4) (Abdollahi *et al.* 2012):

$$\text{Opacity} = \text{Abs}_{600}/X \quad (4)$$

where Abs_{600} is the value of absorbance at 600 nm and X is the film thickness (mm). Samples were cut rectangular and put in the spectrometer cell and the apparatus was calibrated. The light adsorption by film samples was measured at 600 nm wavelength.

Statistical Analysis. To compare the different factors and determine the significant differences of variables, the Duncan test ($P < 0.05$) was used. All the data were reported in mean ± SD.

RESULTS AND DISCUSSION

Nanoparticle and Nanocomposite Characterization Results

Figure 1a shows the XRD patterns of ZnO nanoparticles, which confirms the formation of hexagonal wurtzite structure of ZnO. According to Scherrer equation (Eq. 1), the nanoparticle size was around 36 nm obtained from the peak of (101). The results are in good accordance with the results obtained from the work of Azam *et al.* (2010).

Figure 1b depicts the XRD patterns of PVA/ZnO nanocomposite films with different ZnO concentrations. A wide peak in $2\theta = 19.71°$ in all the samples is attributed to the PVA crystalline structure (Fernandes *et al.* 2011). The small peaks in the patterns of PVA/ZnO nanocomposites verify the incorporation of ZnO nanoparticles in such a way that the intensity increases with the increase of ZnO content (Shivakumaraiah *et al.* 2012).

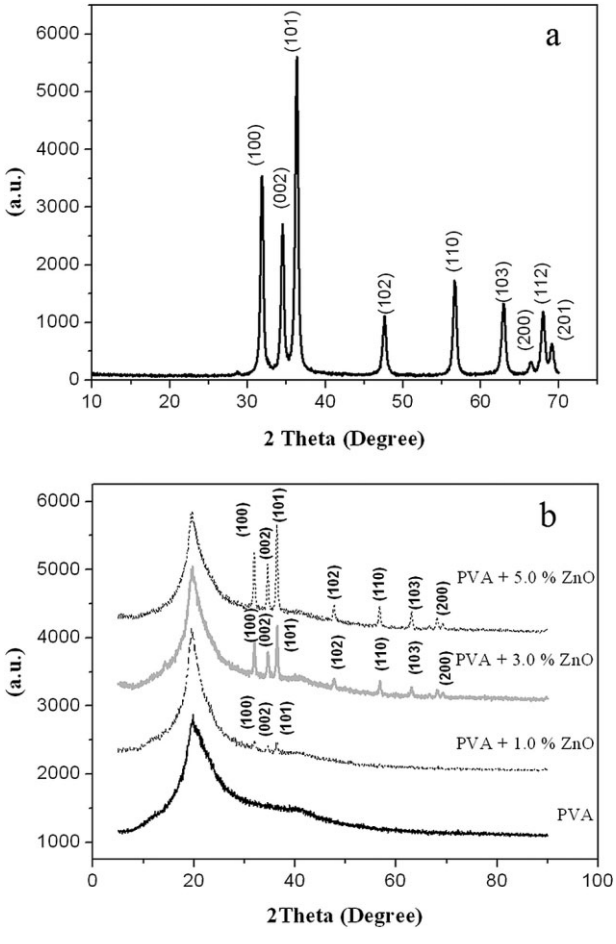

FIG. 1. XRD PATTERN OF THE ZnO POWDER (A) AND THE PVA FILMS (B) WITH ZnO CONCENTRATIONS OF 0, 1, 3 AND 5 WT %

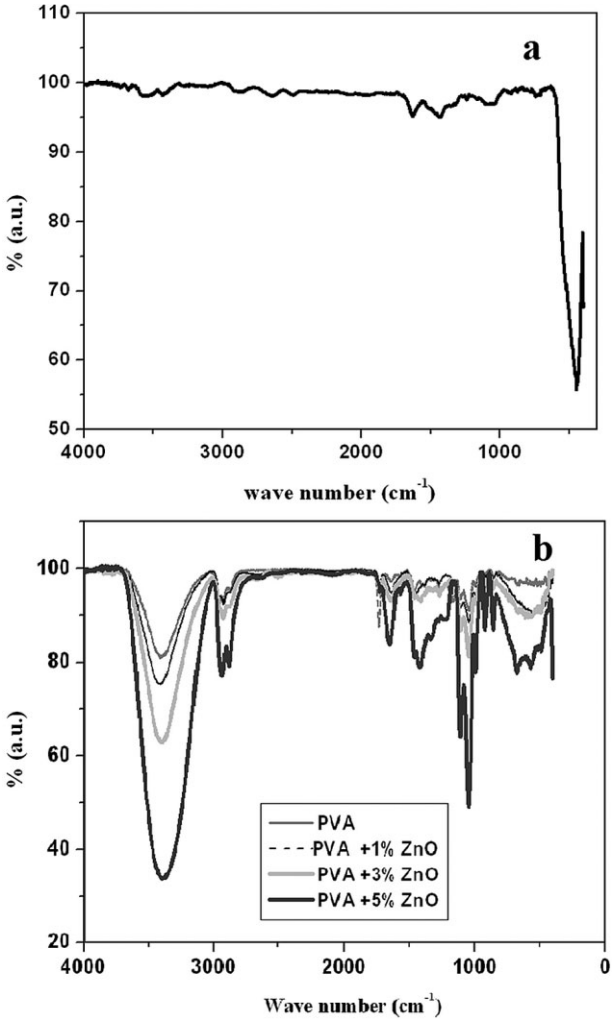

FIG. 2. FTIR SPECTRUM OF THE ZnO POWDER (A) AND THE PVA FILMS (B) WITH ZnO CONCENTRATIONS OF 0, 1, 3 AND 5 WT %

FTIR Analysis

The FTIR spectrum of ZnO nanoparticles is depicted in Fig. 2a. As can be seen, absorption peak in the wave number of 1,633 cm^{-1} could be attributed to the O–H bond of absorbed water on the surface of the sample, while another absorption peak at 1,450 cm^{-1} is related to C–H deformation mode. The peak at 470 cm^{-1} is also due to the Zn–O bond oscillation (Gayan *et al.* 2008; Kumar and Sahare 2012).

Figure 2b depicts the infrared spectrum for PVA film and nanofilms containing ZnO. The existing peaks for PVA and

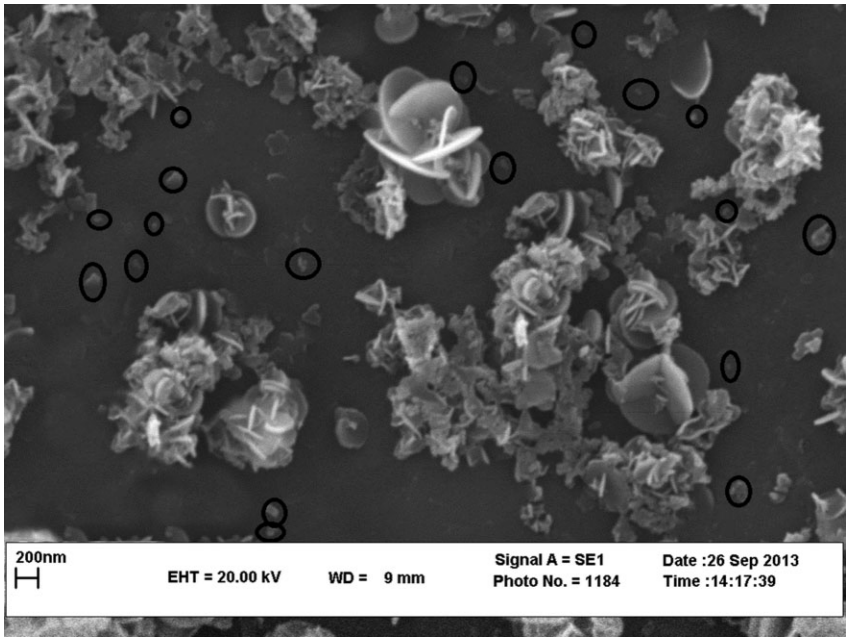

FIG. 3. THE SEM IMAGE OF THE ZnO NANOPARTICLES (IN POWDER FORM) SYNTHESIZED BY SOL-GEL METHOD. THE FLOWERS LIKE OBJECTS ARE AGGLOMERATED NANOPARTICLES. HOWEVER, THE AVERAGE SIZE OF THE ZnO NANOPARTICLES (70 NM) WAS CALCULATED FROM NONAGGLOMERATED PARTICLES WHICH ARE HIGHLIGHTED WITH BLACK CIRCLES

the nanocomposite films at wave number of 3,300 cm^{-1} are due to O–H groups. The peaks between 2,852 and 2,918 cm^{-1} are the symmetric and asymmetric C–H_2 bond's osculation, respectively, while the peaks at 1,413 cm^{-1} is due to C–C bond. Moreover, the peak at about 558 cm^{-1} for PVA and ZnO nanocomposites is indicative of Zn–O bond which verifies the presence of ZnO nanoparticles in the PVA matrix. The switching of peak from 470 cm^{-1} in ZnO to 558 cm^{-1} in nanocomposite might be related to the interactions between ZnO particles and PVA. It is seen that by increase of ZnO nanoparticle concentration, these peaks increased as reported by Roy *et al.* (2013). A band at 1,080 cm^{-1} corresponds to C–O–C stretching of acetyl group present on PVA backbone (Xue and Wei 2009).

Morphology Analysis

Figure 3 illustrates the SEM image of nanoparticle samples. It is clearly seen that the samples possess the flower-like surface morphology with the average size of 70 nm. Because of the high surface energy of the samples, they have the tendency to agglomerate and form the larger particles. Therefore, the average size of particles is larger than the results obtained from Scherrer equation (Rajamanickam *et al.* 2013).

The TEM image of nanoparticles is also shown in Fig. 4a.The size of particles ranged from 18 to 85 nm and they showed a relatively spherical geometry. This shows a good agreement with the results obtained from particle size analyzer in which the average size of particles is approximately 40 nm (Fig. 4b).

SEM Images

The SEM images of the nanocomposite films with different ZnO contents are shown in Fig. 5. As can be seen, the ZnO nanoparticles are evenly distributed in the polymer matrices and no cracks are observable in the films (polymer matrices). Because of the high surface energy, excessive nanoparticles were easily agglomerated. The results are in good accordance with the results obtained from the work of Lee *et al.* (2008).

Mechanical Properties

Figure 6 shows the effect of ZnO nanoparticle concentration and nanofilm thickness on E%, TS and YM at the weak point of films. As shown in this figure, the pure PVA at different thicknesses had the least TS and YM, while its strain percent at weak point was the highest. As expected for all treatments with thickness increment, the TS and YM increased. With the increase of ZnO nanoparticle concentration up to 3% in the PVA, the increases in TS and YM were significant ($P < 0.05$) about 64 and 72%, respectively, while in the case of 5% ZnO concentration, these amounts showed a reduction. It may be the result of an increase in nanoparticle agglomeration, which is also confirmed with nanocomposite surface view in Fig. 5. This can be concluded that as long as the nanoparticle concentration is such that the nanomaterials are sufficiently distributed within the PVA with homogenous structure, the mechanical properties can be modified by ZnO nanoparticle insertion as also reported by Li *et al.* (2009a,b). The highest tensile strength

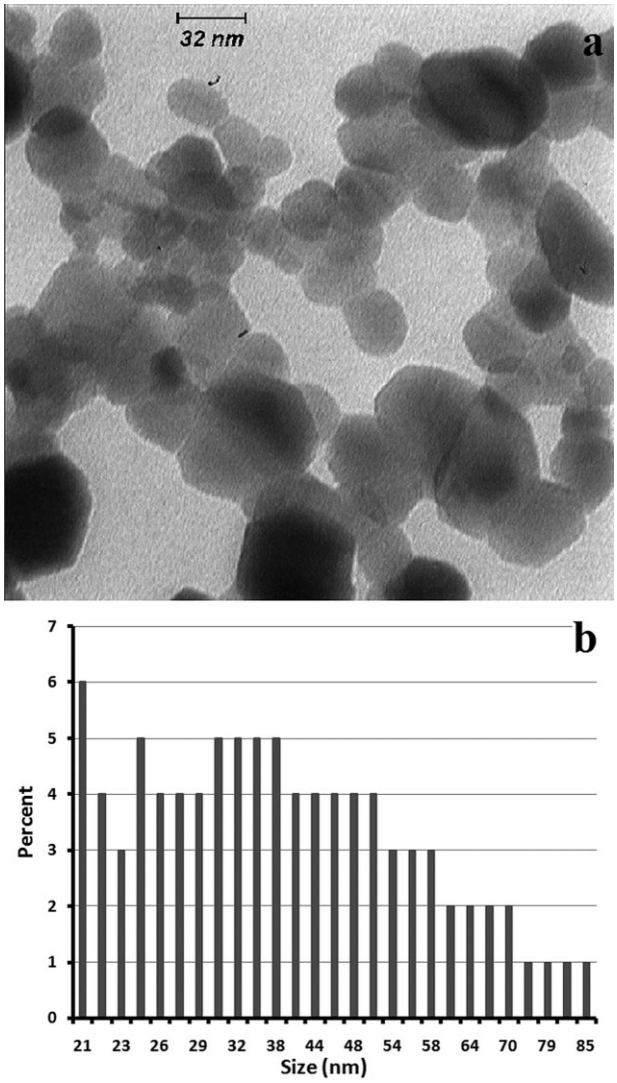

FIG. 4. TEM IMAGE (A) AND HISTOGRAM OF ZnO NANOPARTICLE SIZE DISTRIBUTION (B) SYNTHESIZED BY SOL-GEL METHOD

was achieved at around 130 μm of film thickness and 3% nanoparticle concentration. The decrease of E% with the increase of ZnO concentration may be due to the rough nature of filler (Pereda *et al*. 2011). In other words, the combination of ZnO limits the movement of PVA bed in terms of the strong interactions between the fillers and polymer matrix (Cao *et al*. 2008).

Water Vapor Penetration Properties (WVP)

WVP is one of the most important parameters for biodegradable films. Vapor penetration to the pure PVA and nanocomposites with different concentrations of nano-ZnO and with different thicknesses is shown in Fig. 7. By adding the nanoparticles and increasing the film thickness, the WVP of the film decreased ($P < 0.05$). Most of the reduction in gas penetration was observed in the case of thickness of 130 μm and the ZnO concentration of 5%. In such treatment, the WVP of the film decreased by 39%. The vapor penetration reduction is due to incorporation of nanoparticles because it would result in a more complicated path for oxygen and other gases to penetrate (Yu *et al*. 2009). Nafchi *et al*. (2012) reported similar results for vapor permeation after incorporation of nanoparticles.

Moreover, the results of this study confirmed the previous results obtained by Yu *et al*. (2009) and Nafchi *et al*. (2012) which expressed that by increasing the film's thickness, the vapor penetration shows a reduction.

Antibacterial Properties of Nanocomposites

The antibacterial properties of nanocomposites are shown as inhibition zone against *E. coli* in Table 1. By introduction of ZnO nanoparticles to PVA, and with increase in the nanofilm thickness, the bacteria natural growth was slowed down sufficiently and the bacteria growth inhibition intensified ($P < 0.05$). Bacteria growth inhibition in the pure PVA at all concentrations was zero. Hence, it can be said that the presence of ZnO nanoparticles in the PVA matrix enhances the bacteria growth inhibition. Nafchi *et al*. (2012) observed that the growth of *Staphylococcus aureus* was affected significantly by ZnO-coated films compared to control films. The antibacterial activity of WPU/f-ZnO composite films against *E. coli* and *S. aureus* was also tested. The results revealed that the antibacterial activity enhanced with the increase of f-ZnO content, and the best antibacterial activity was obtained (Xue and Wei 2009). Espitia *et al*. (2013) indicated that ZnO nanoparticles incorporated in pediocin films exhibited excellent antibacterial activity against *S. aureus* and *Listeria monocytogenes*. Mechanisms of the antibacterial behavior of ZnO have been detailed by Zhang *et al*. (2010). They have categorized this behavior as chemical and/or physical interaction between ZnO particles and the cell envelope of microorganism. The Zn^{2+} penetrated into the microorganisms' cell walls and reacted with internal materials. The antibacterial phenomena may also be due to hydrogen peroxide production from the surface (Zhang *et al*. 2010). They also reported that the nanosize of ZnO is more effective than the microsize due to easy penetration through cell walls of microorganisms. Sawai (2003) also reported the same results and demonstrated that among ZnO, CaO and MgO, the former was the most effective for *S. aureus* compared to *E. coli*.

Color and Transparency

The color and transparency of films are important in the food packaging appearance and customer acceptance and

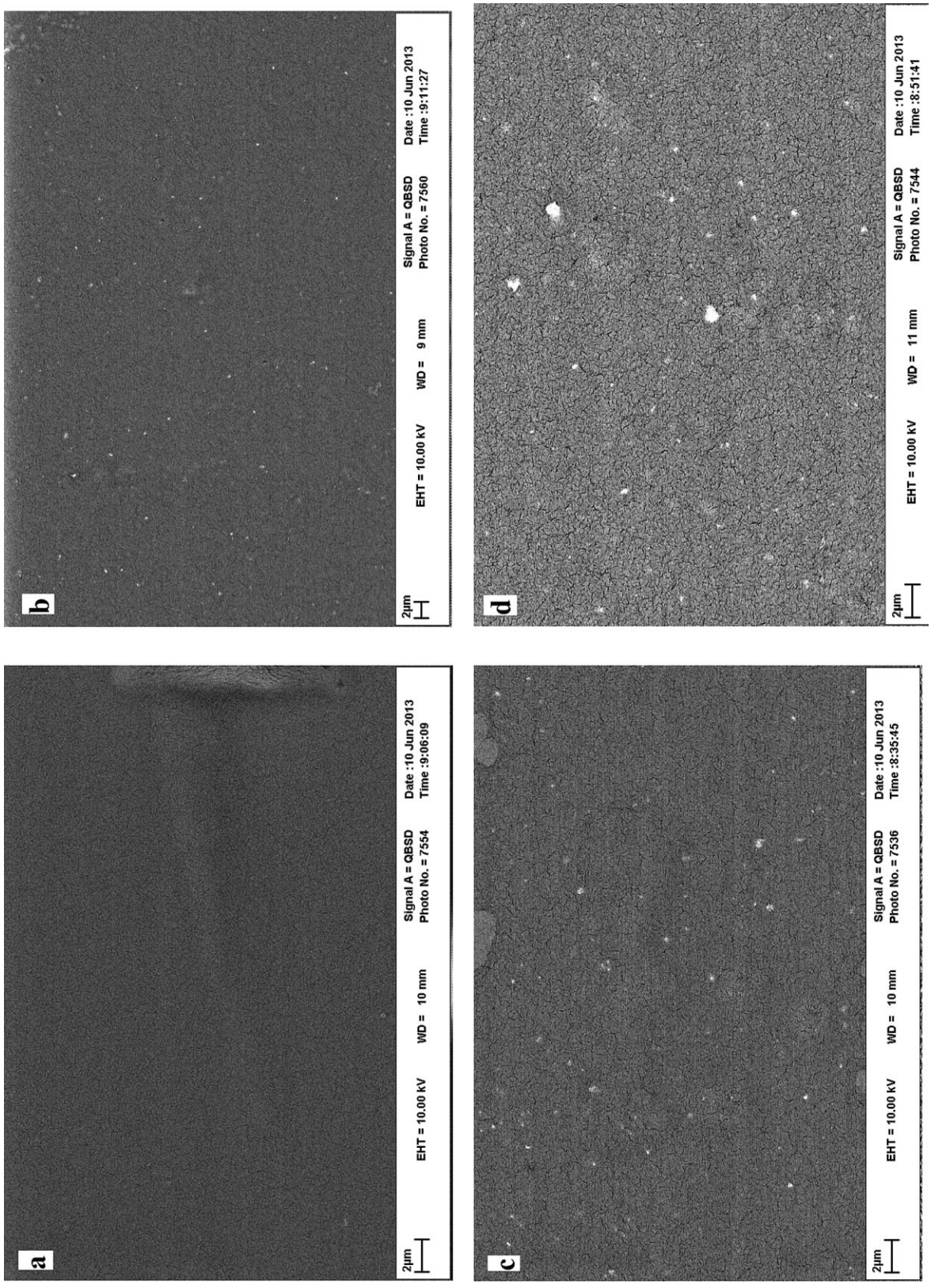

FIG. 5. SEM IMAGES OF (A) PVA WITH NO ZnO CONTENT, (B) PVA/1% ZnO, (C) PVA/3% ZnO AND (D) PVA/5% ZnO

satisfaction (Rao *et al.* 2010). The amounts of L^*, a^*, b^* and ΔE in the pure PVA and nanofilm with different nano-ZnO concentrations and different thicknesses are shown in Table 1. It can be seen that by addition of ZnO from 1 to 5%, L^* increased ($P < 0.05$). Nafchi *et al.* (2012) showed that the nanofilms containing starch had different results in comparison with the ZnO containing films. The values of L^* and ΔE also increased by increasing the thickness ($P < 0.05$).

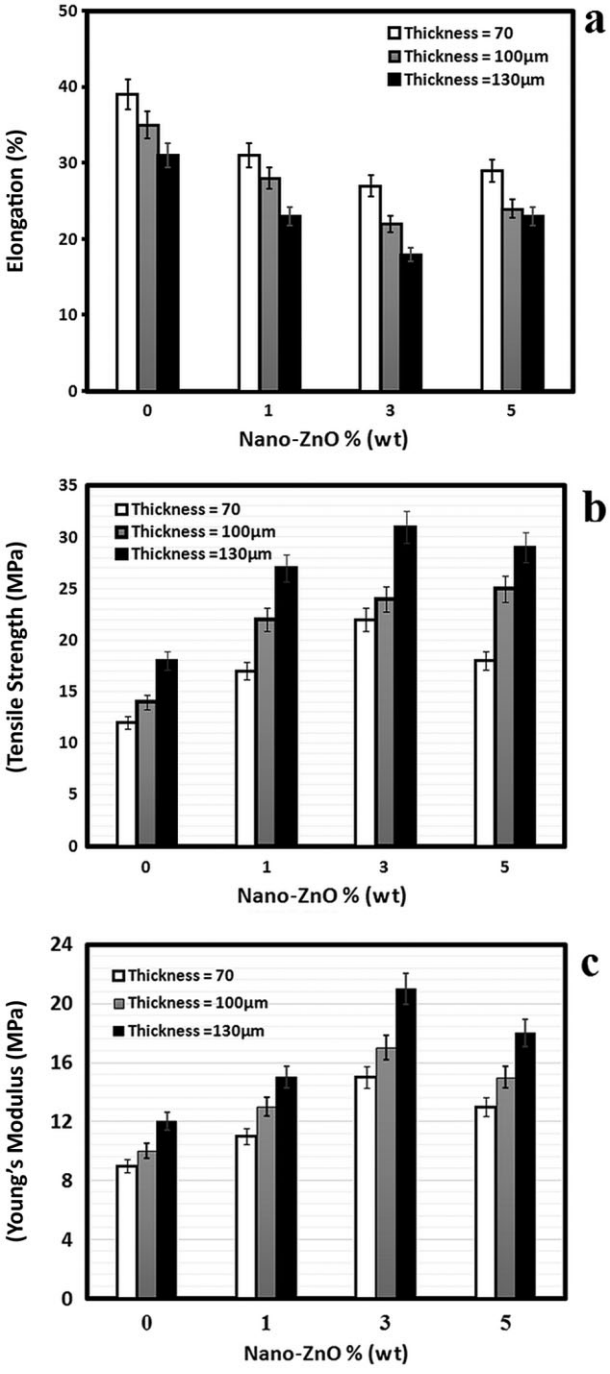

FIG. 6. ELONGATION (A), TENSILE STRENGTH (B) AND YOUNG'S MODULUS (C) OF PVA FILMS WITH DIFFERENT CONCENTRATIONS OF ZnO (0, 1, 3 AND 5 WT %). ERROR BARS REPRESENT STANDARD DEVIATION AND INDICATE SIGNIFICANT DIFFERENCE AT $P < 0.0$

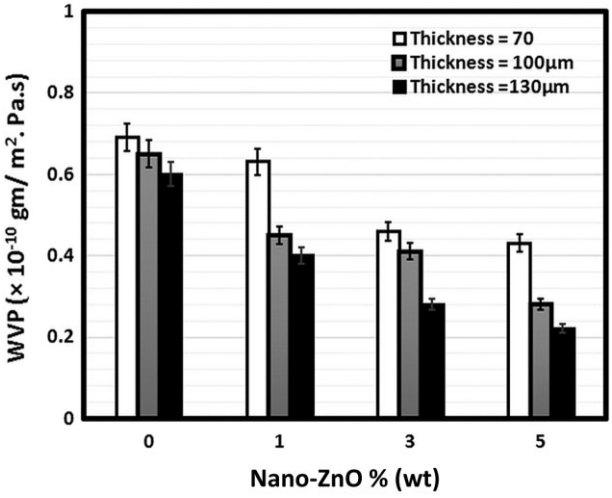

FIG. 7. WVP OF PVA/ZnO NANOCOMPOSITE FILM

Opacity is used for film transparency determination. With opacity increment, the transparency decreases (Pereda *et al.* 2011). Based on Table 1, the opacity of pure PVA film was the lowest so it had the highest transparency. The increase in nanoparticle concentration and thickness of the films led to increase in its opacity. Because PVA is a transparent material, the reduction in PVA transparency could be the result of nanoparticle agglomeration in the polymer matrix, which was confirmed with SEM and the analysis of mechanical and vapor penetration properties. The decrease of film transparency by addition of nanoparticles was also reported by Abdollahi *et al.* (2012).

CONCLUSIONS

Sol-gel-derived ZnO nanoparticles and PVA nanocomposites were successfully prepared by solution casting method. The XRD tests TEM and SEM showed that ZnO nanoparticles were synthesized with appropriate structure. The infrared spectrometry confirmed the presence of ZnO in PVA matrix. Furthermore, the nanofilm structural analysis showed that ZnO nanoparticles were homogenously distributed in the polymer bed with good intercalation in polymer strings. Moreover, it was seen that by adding ZnO nanoparticles to the PVA, the mechanical properties of nanocomposites were modified. By incorporation of nanoparticles into PVA matrices, the vapor penetration was decreased and barrier properties were promoted. Moreover, PVA/ZnO nanocomposites showed a good antibacterial

TABLE 1. COLOR, OPACITY AND ANTIBACTERIAL ACTIVITY OF DIFFERENT TREATMENTS OF PVA/ZnO NANOCOMPOSITES

(ZnO) %	Thickness (μm)	*L**	*a**	*b**	Δ*E*	Opacity	Antibacterial (×10³ mm²)
0	70 ± 2	45.39 ± 2.23^{a}	–4.78 ± 0.85^{d}	21.89 ± 1.18^{b}	50.88 ± 1.22^{g}	1.15 ± .08^{a}	0 ± 0^{a}
0	100 ± 3	55.77 ± 1.26^{b}	–4.79 ± 0.84^{d}	24.74 ± 2.37^{a}	46.39 ± 2.37^{f}	1.46 ± 0.24^{b}	0 ± 0^{a}
0	130 ± 2	60.57 ± 1.74^{b}	–5.14 ± 0.37^{cd}	25.78 ± 2.13^{a}	44.79 ± 0.16^{f}	1.81 ± 0.06^{c}	0 ± 0^{a}
1	70 ± 2	57.46 ± 1.74^{b}	–6.54 ± 0.86^{a}	18.50 ± 2.20^{cd}	42.71 ± 1.78^{f}	2.81 ± 0.14^{d}	1.71 ± 0.29^{b}
1	100 ± 2	66.13 ± 1.48^{d}	–6.26 ± 1.12^{ab}	21.24 ± 2.09^{bc}	36.30 ± 2.01^{e}	2.99 ± 0.06^{d}	1.76 ± 0.47^{a}
1	130 ± 1	70.74 ± 0.74^{e}	–5.04 ± 0.22^{cd}	16.64 ± 1.54^{d}	30.01 ± 1.39^{d}	3.68 ± 0.13^{e}	2.52 ± 0.12^{a}
3	70 ± 5	71.75 ± 1.38^{e}	–6.26 ± 0.42^{abc}	17.06 ± 0.65^{d}	29.45 ± 1.55^{d}	5.29 ± 0.07^{f}	7.74 ± 0.59^{c}
3	100 ± 3	77.69 ± 0.32^{f}	–4.70 ± 0.49^{d}	20.75 ± 0.91^{bc}	27.56 ± 0.46^{cd}	5.73 ± 0.03^{g}	8.54 ± 0.16^{c}
3	130 ± 1	85.30 ± 1.64^{g}	–5.04 ± 0.76^{cd}	19.17 ± 1.09^{bcd}	26.67 ± 1.48^{bc}	6.44 ± 0.09^{h}	8.95 ± 0.21^{c}
5	70 ± 2	79.10 ± 0.36^{f}	–4.89 ± 0.11^{d}	20.67 ± 1.15^{bc}	23.36 ± 0.99^{abc}	6.45 ± 0.07^{h}	10.41 ± 0.03^{d}
5	100 ± 3	79.74 ± 1.47^{f}	–6.14 ± 0.14^{abc}	16.71 ± 0.94^{d}	22.32 ± 0.30^{ab}	6.54 ± 0.07^{h}	11.33 ± 0.42^{de}
5	130 ± 4	85.78 ± 1.39^{g}	–5.65 ± 0.20^{abcd}	16.99 ± 0.57^{d}	20.32 ± 1.03^{a}	6.82 ± 0.10^{i}	12.43 ± 0.42^{e}

property, thus these films can be used as antibacterial food packaging materials.

REFERENCES

ABDOLLAHI, M., REZAEI, M. and FARZI, G. 2012. A novel active bionanocomposite film incorporating rosemary essential oil and nanoclay into chitosan. J. Food Eng. *111*, 343–350.

ABDOLLAHI, M., ALBOOFETILEH, M., BEHROOZ, R., REZAEI, M. and MIRAKI, R. 2013. Reducing water sensitivity of alginate bio-nanocomposite film using cellulose nanoparticles. Int. J. Biol. Macromol. *54*, 166–173.

ALBOOFETILEH, M., REZAEI, M., HOSSEINI, H. and ABDOLLAHI, M. 2013. Effect of montmorillonite clay and biopolymer concentration on the physical and mechanical properties of alginate nanocomposite film. J. Food Eng. *117*, 26–33.

ARORA, A. and PADUA, G.W. 2010. Review: Nanocomposites in food packaging. J. Food Sci. *75*, 43–49.

ASTM 2002. http://www.astm.org/DATABASE.CART/HISTORICAL/D882-02.htm (accessed December 21, 2002).

AZAM, A., AHMED, F., ARSHI, N., CHAMAN, M. and NAQVI, A.H. 2010. Formation and characterization of ZnO nanopowder synthesized by sol-gel method. J. Alloys Compd. *496*, 399–402.

CAO, X., CHEN, Y., CHANG, P.R., STUMBORG, M. and HUNEAULT, M.A. 2008. Green composites reinforced with hemp nanocrystals in plasticized starch. J. Appl. Polym. Sci. *109*, 3804–3810.

CHANDRAKALA, H.N., RAMARAJ, B., MADHU, G.M., SHIVAKUMARAIAH and SIDDARAMAIAH. 2012. The influence of zinc oxide cerium oxide nanoparticles on the structural characteristics and electrical properties of polyvinyl alcohol films. J. Mater. Sci. *42*, 8076–8084.

CHAUDHRY, Q., SCOTTER, M., BLACKBURN, J., ROSS, B., BOXALL, A. and CASTLE, L. 2008. Applications and implications of nanotechnologies for the food sector. Food Addit. Contam. Part A Chem. Anal. Control Expo. Risk Assess. *25*, 241–258.

DASTJERDI, R. and MONTAZER, M. 2010. A review on the application of inorganic nano-structured materials in the modification of textiles: Focus on anti-microbial properties. Colloids Surf. B. Biointerfaces *79*, 5–18.

ESPITIA, P.J.P., SOARES, N.F.F., TEOFILO, R.F., COIMBRA, J.S.R., VITOR, D.M., BATISTA, R.A., FERREIRA, S.O., ANDRADE, N.J. and MEDEIRO, E.A.A. 2013. Physical-mechanical and antimicrobial properties of nanocomposite films with pediocin and ZnO nanoparticles. Carbohydr. Polym. *94*, 199–208.

FERNANDES, D.M., WINKLER HECHENLEITNER, A.A., LIMA, S.M., ANDRADE, H.L.C., CAIRES, A.R.L. and GÓMEZ PINEDA, E.A. 2011. Preparation, characterization, and photoluminescence study of PVA/ZnO nanocamposite films. Mater. Chem. Phys. *128*, 371–376.

GAYAN, R.N., DAS, S.N., DALUI, S., BHAR, R. and PAL, A.K. 2008. Zinc magnesium oxide nanofibres on glass substrate by solution growth technique. J. Cryst. Growth *310*, 4073–4080.

KOMPANY, A., MADAHI, P., SHAHTAHMASSBI, N. and MASHREGHI, M. 2012. Synthesis, characterization and antibacterial property of ZnO: Mg nanoparticles. AIP Conference Proceedings, USA.

KUMAR, S. and SAHARE, P.D. 2012. Observation of band gap and surface defects of ZnO nanoparticles synthesized via hydrothermal route at different reaction temperature. Opt. Commun. *285*, 5210–5216.

LEE, J., BHATTACHARYYA, D., EASTEAL, A.J. and MESTON, J.B. 2008. Properties of nano- ZnO/poly (vinyl alcohol)/ poly (ethylene oxide) composite thin film. Curr. Appl. Phys. *8*, 42–47.

LEE, J., EASTEAL, A.J., PAL, U. and BHATTACHARYYA, D. 2009. Evolution of ZnO nanostructures in sol-gel synthesis. Curr. Appl. Phys. *9*, 792–796.

LI, J.H., HONG, R.Y., LI, M.Y., LI, H.Z., ZHENG, Y. and DING, J. 2009a. Effects of ZnO nanoparticles on the mechanical and antibacterial properties of polyurethane coatings. J. Pro. Org. Coat *64*, 504–509.

LI, Q., ZHOU, J. and ZHANG, L. 2009b. Structure and properties of the nanocomposite films of chitosan reinforced with cellulose whiskers. J. Polym. Sci. *47*, 1069–1077.

LIVAGE, J., HENRY, M. and SACHEZ, C. 1988. Sol-gel-chemistry transition metal oxide. Prog. Solid State Chem. *18*, 258–341.

NAFCHI, A.M., ALIAS, A.K., MAHMUD, S. and ROBAL, M. 2012. Antimicrobial, rheological, and physicochemical properties of sago starch films filled with nanorod-rich zinc oxide. J. Food Eng. *113*, 511–519.

NAIR, M.G., NIRMALA, M., REKHA, K. and ANUKALIANI, A. 2011. Structural, optical, photo catalytic and antibacterial activity of ZnO and Co doped ZnO nanoparticles. Mater. Lett. *65*, 1797–1800.

PEREDA, M., AMICA, G., RACZ, I. and MARCOVICN, N.E. 2011. Structure and properties of nanocomposite films based on sodium caseinate and nanocellulose fibers. J. Food Eng. *103*, 76–83.

RAJAMANICKAM, N., RAJASHABALA, S. and RAMACHANDRAN, K. 2013. Theoretical and experimental investigation on enhance thermal behavior in chunk-shaped nano ZnO. Mol. Phys. *112*, 142–150.

RAO, M.S., KANATT, S.R., CHAWLA, S.P. and SHARMA, A. 2010. Chitosan and guar gum composite films preparation: physical, mechanical and antibacterial properties. Carbohydr. Polym. *82*, 1243–1247.

ROY, A.S., GUPTA, S., SINDHU, S., PARVEEN, A. and RAMAMURTHY, P.C. 2013. Dielectric properties of novel PVA/ZnO hybrid nanocomposite films. Compos. Part B Eng. *47*, 314–319.

SAWAI, J. 2003. Quantitative evaluation of antibacterial activities of metallic oxide powders (ZnO, MgO and CaO) by conductimetric assay. J. Microbiol. Methods *54*, 177–182.

SAWAI, J., SHOJI, S., IGRASHI, H., HASHIMOTO, A., KOKUGAN, T., SHIMIZ, M. and KOJIMA, H. 1998. Hydrogen peroxide as an antibacterial factor in zinc oxide powder slurry. J. Ferment. Bioeng. *86*, 521–522.

SEDAGHAT, N. and ZAHEDI, Y. 2012. Application of edible coating and acidic washing for extending the storage life of mushrooms (*Agaricus bisporus*). Food Sci. Technol. Int. *18*, 523–530.

SHALL, M.S.E., GRAIVER, D. and PERNISZ, U. 1995. Synthesis and characterization of nanoscale zinc oxide particles: l. laser vaporization/condensation technique. Nanostruct. Mater. *6*, 297–300.

SHIVAKUMARAIAH, H.N.C., SIDDARAMAIAH, H.N.C., RAMARAJ, B. and MADHU, G.M. 2012. The influence of zinc oxide – cerium oxide nanoparticles on the structural characteristics and electrical properties of polyvinyl alcohol films. J. Mater. Sci. *47*, 8076–8084.

SORRENTINO, A., GORRASI, G. and VITTORIA, V. 2007. Potential perspective of bio-nanocomposites for food packaging applications. Trends Food Sci. Technol. *18*, 84–95.

SUCHANEK, W.L. 2009. Systematic study of hydrothermal crystallization of zinc oxide (ZnO) nano – sized powder with superior UV attenuation. J. Cryst. Growth *312*, 100–108.

TANKHIWALE, R. and BAJPAI, S.K. 2012. Preparation, characterization and antibacterial applications of ZnO-nanoparticles coated polyethylene films for food packaging. Colloids Surf. B. Biointerfaces *90*, 16–20.

THARANATHAN, R.N. 2003. Biodegradable films and composite coatings: Past, present and future. Trends Food Sci. Technol. *14*, 71–78.

VAIDYA, U.R. and BHATTACHARYA, M. 1994. Properties of blends of starch and synthetic polymers containing anhydride groups. J. Appl. Polym. Sci. *52*, 617–628.

XUE, Y.M. and WEI, D.Z. 2009. Effects of flower- like ZnO nanowhiskers on the mechanical, thermal and antibacterial properties of waterborne polyurethane. Polym. Degrad. Stab. *94*, 1103–1109.

YU, D., CAI, R. and LIU, Z. 2009. Preparation and characterization of glycerol plasticized- pea starch/ZnO-carboxymethylecellulose sodium nanocomposites. Bioresour. Technol. *100*, 2832–2841.

ZHANG, L., JIANG, Y., DING, Y., DASKALAKIS, N., JEUKEN, L., POVEY, M., NEILL, A.Ó. and YORK, D. 2010. Mechanistic investigation info antibacterial behavior of suspensions of ZnO nanoparticles against E. coli. J. Nanopart. Res. *12*, 1625–1636.